Processing and Application of Ceramics 11 [1] (2017) 60–66
DOI: 10.2298/PAC1701060V

Effect of cobalt substitution on structural, electrical and magnetic properties of $NiFe_2O_4$

Kannipamula Vijaya Babu[1,*], Matangi Ravi Chandra[1], Gondu Venkata Santosh Kumar[1], Kantamsetti Jagadeesh[2]

[1]*Advanced Analytical Laboratory, Andhra University, Visakhapatnam-530 003, India*
[2]*Sri Vasavi Engineering College, Tadepalligudem, Andhra Pradesh, India*

Received 13 October 2016; Received in revised 24 January 2017; Accepted 1 March 2017

Abstract

Nickel ferrite and cobalt substituted nickel ferrite were synthesized by sol-gel method using citric acid as chelating reagent. X-ray diffraction revealed the formation of nanocrystalline particles having spinel structure with space group Fd3m. FTIR spectra showed fundamental absorption bands in the range 400–1300 cm^{-1}, related to iron ions on both octahedral and tetrahedral sites which are typical for ferrite structure. SEM analyses confirmed that the particles are agglomerated with an average size of about 1.5 μm. The ferrite powders were pressed at 5 MPa and sintered at 1200 °C for 5 h. Conductivities, impedance analyses and dielectric properties of $NiFe_2O_4$ and $Ni_{0.7}Co_{0.3}Fe_2O_4$ ceramics were investigated over the frequency range of 20 Hz to 1 MHz at room temperature. The obtained experimental results are in good agreement with the reported values.

Keywords: *nickel ferrite, structural characterization, electrical properties*

I. Introduction

In the last few decades tremendous development has been made in the field of nanotechnology, particularly in materials science. Ferrites are important magnetic materials in technological and industrial applications owing to their combination of electrical and magnetic properties. They possess low electrical conductivity, high saturation magnetization, high permeability, low eddy current, dielectric loss and other properties which makes them usable in different applications. Ferrites with such combination of electrical insulator and magnetic conductor are important magnetic materials which are irreplaceable by any other magnetic materials. The nano-sized ferrites have been attracting extensive attention due to their wide applications, such as magnetic memory, MRI contrasts agents, efficient hyperthermia for cancer therapy and catalysts [1]. The advantages of nano-ferrites are due to their higher efficiency and lower cost and ease of manufacturing than other materials [2–4]. On the basis of crystal structure ferrites are separated in three types namely, hexagonal ferrite, garnet and spinel ferrite. Spinel ferrites have the general formula MFe_2O_4 in which M and Fe are in tetrahedral and octahedral cation sites, respectively, and O is in the oxygen anion site. They are also called cubic ferrites. According to distribution of cations, spinel ferrites are classified in to three types; random spinel, normal spinel and inverse spinel. Among these ferrites, the inverse type ferrite is more interesting due to its high magneto crystalline anisotropy and high saturation magnetization. In the inverse type ferrites, half of the trivalent ions occupy A-sites and the other half of the trivalent cations and total divalent cations randomly occupy B-sites. Nickel ferrite ($NiFe_2O_4$) is one of the most important materials in the inverse spinel family. Nickel ferrite and substituted nickel ferrites have been widely studied because of their typical ferromagnetic properties, low conductivity, high electrochemical stability high mechanical hardness and low cost [5,6].

The method of preparation plays an important role in the properties of the ferrite nanoparticles. Generally, ferrites are highly sensitive to preparation method, sintering conditions, amount of constituent metal oxides, various additives included as dopants and impurities [7]. Large number of methods is available for the synthesis of ferrites; the most commonly used method is solid

* Corresponding author: +91 891 2844741,
fax: +91 891 2844742, e-mail: *vijayababu.k@gmail.com*

state reaction method for bulk ferrites. Various chemical routes have been already adopted by many researchers to synthesize nanocrystalline $NiFe_2O_4$ powders including co-precipitation [8], hydrothermal [9], auto combustion [10], sol-gel [11,12] and reverse micelle methods. Among them sol-gel method is an attractive way for producing nano-ferrite powders because of its cost effectiveness, homogeneity, purity and reactivity [13,14].

In the present paper, we have used the sol-gel method due to its low cost and tailor made synthesis conditions. It is very simple method to provide homogeneous powder. $NiFe_2O_4$ and $Ni_{0.7}Co_{0.3}Fe_2O_4$ nanoparticles are prepared successfully by the sol-gel method and sintered at 1200 °C. The lattice parameter, structural morphology, dielectric and magnetic properties of the nanocrystalline powders are systematically studied. The obtained results are well compared with previous literature and encouraging for further studies.

II. Experimental

The $NiFe_2O_4$ and $Ni_{0.7}Co_{0.3}Fe_2O_4$ nano-ferrite powders were prepared from nickel nitrate ($Ni(NO_3)_2{\times}6\,H_2O$), cobalt nitrate ($Co(NO_3)_2{\times}6\,H_2O$), ferric nitrate ($Fe(NO_3)_3{\times}9\,H_2O$) and citric acid ($C_6H_8O_7$) by sol-gel auto-combustion method. The molar metal nitrates to citric acid ratio was taken as 1 : 3. Ammonia solution was added to maintain the pH at 7. The collected compounds were then dried in oven for 2 hours. The powder samples, mixed with polyvinyl alcohol (PVA) as a binder, were ground and then pressed at 5 MPa/6 min into a circular disk shaped pellets (with thickness of 1 mm and diameter of 10 mm). The synthesized powders and pellets were heat treated (sintered) at 1200 °C for 5 hours and then used for further investigations.

The prepared nano-ferrites $NiFe_2O_4$ and $Ni_{0.7}Co_{0.3}Fe_2O_4$ samples were characterized by standard techniques, such as X-ray diffraction (XRD), scanning electron microscope (SEM), electron spin resonance (ESR) and LCR meter. The XRD patterns were recorded at room temperature in the 2θ range of 10° to 70° using Cu-Kα radiation (λ = 1.5405 Å). The particle morphology of the powders was observed using scanning electron microscopy images taken by JEOL JSM-6610L. The magnetic properties were measured using JEOL electron spin resonance (ESR). Before impedance measurements the pellets were polished by fine emery paper to make their faces smooth and parallel and finally coated with conductive silver paint. The impedance study was performed by Wayne-Kerr high frequency Network Analyzer Model 65120 in the frequency range 20 Hz to 1 MHz at room temperature.

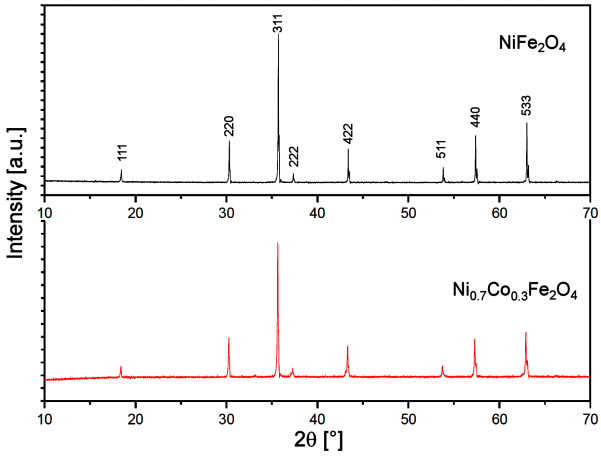

Figure 1. X-ray diffraction patterns of $NiFe_2O_4$ and $Ni_{0.7}Co_{0.3}Fe_2O_4$ calcined powders

III. Results and discussion

3.1. Structural characterization

X-ray diffraction patterns were taken at room temperature to confirm the crystal structure of the obtained particles. All the reflections seen in the XRD patterns (Fig. 1) are sharp, clear and intense, confirming the spinel phase. The peaks match well with characteristic reflection of $NiFe_2O_4$ (JCPDS card number 89-4927) and correspond to the planes (220), (311), (222), (400), (422) (511), (440) and (533) indexed using Bragg's law indicating the presence of cubic spinel with space group *Fm3m*. The lattice parameter and unit cell volume of $NiFe_2O_4$ and $Ni_{0.7}Co_{0.3}Fe_2O_4$ ferrites were calculated using unit cell software and given in Table 1. An increase in parameter from 8.3323 Å ($NiFe_2O_4$) to 8.3442 Å ($Ni_{0.7}Co_{0.3}Fe_2O_4$) is noticed. The difference in lattice parameter is due to difference in ionic radii of Co^{2+} (0.745 Å) and Ni^{2+} ion (0.69 Å) [15,16]. The crystallite sizes of both ferrites were estimated from the full width at half maximum (FWHM) of the most intense 311 peak and by Scherer's equation. The crystallite size increases from 14.8 nm to 17.8 nm with cobalt substitution. Table 1 also includes the values of molecular weight (M) and cell volume (V). Miller indices (hkl) and inter-planar spacing (d) of $NiFe_2O_4$ and $Ni_{0.7}Co_{0.3}Fe_2O_4$ are listed in Table 2 [17]. Our results are in good agreement with that reported in the literature.

Figure 2 represents the Fourier transform infrared (FTIR) spectra of $NiFe_2O_4$ and $Ni_{0.7}Co_{0.3}Fe_2O_4$ ferrite powders. It is well known that normal and inverse cubic spinels have two fundamental absorption bands - the first band is due to tetrahedral and the second is due to octahedral complexes. The FTIR spectra shows two

Table 1. Lattice parameter (a), volume (V), crystallite size and molecular weight of $NiFe_2O_4$ and $Ni_{0.7}Co_{0.3}Fe_2O_4$

Type of ferrite	Lattice parameter [Å]	Volume [Å^3]	Crystallite size [nm]	Molecular weight [g/mol]
$NiFe_2O_4$	8.3323	578.5	14.8	234.38
$Ni_{0.7}Co_{0.3}Fe_2O_4$	8.3442	581.0	17.8	234.47

Table 2. Miller indices (*hkl*) and inter-planar spacing (*d*) of $NiFe_2O_4$ and $Ni_{0.7}Co_{0.3}Fe_2O_4$

hkl	*d*-spacing [Å]	
	$NiFe_2O_4$	$Ni_{0.7}Co_{0.3}Fe_2O_4$
1 1 1	4.8068	4.8172
2 2 0	2.9458	2.9512
3 1 1	2.5124	2.5171
2 2 2	2.4054	2.4097
4 2 2	2.0837	2.0872
5 1 1	1.7019	1.7044
4 4 0	1.6046	1.6070
5 3 3	1.4740	1.4762

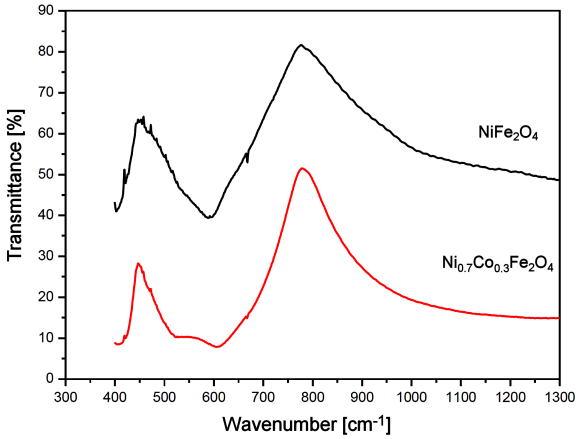

Figure 2. FTIR spectra of $NiFe_2O_4$ and $Ni_{0.7}Co_{0.3}Fe_2O_4$ calcined powders

main absorption bands of the iron ions on both tetrahedral and octahedral positions υ_1 and υ_2 in the range of 774–779 cm^{-1} and 445–452 cm^{-1}, respectively. From Fig. 2 it can be observed that the υ_1 and υ_2 shifted slightly due to cobalt substitution in $NiFe_2O_4$. The difference in the band positions for tetrahedral and octahedral complexes is due to the difference in values of Fe^{3+}–O^{2-} band distances. The higher frequency absorption band υ_1 is assigned to vibrations of the tetrahedral metal complexes which is the bond between the oxygen ion and tetrahedral site metal ion. Lower frequency band υ_2 is assigned to vibration of octahedral metal complexes which is the bond between oxygen ion and octahedral site metal ion. The existence of these two bands υ_1 and υ_2 reveals that these samples are single phase spinel ferrites [18–20]. In the present study the absorption bands of both ferrites under investigation were found to be in the reported range.

The SEM images of $NiFe_2O_4$ and $Ni_{0.7}Co_{0.3}Fe_2O_4$ ferrite powders are shown in Fig. 3. It is clearly observed that the powders are agglomerated, highly branched and porous in nature. The average grain sizes of both ferrites are 1.25 and 1.74 μm, respectively. The average grain size of the samples obtained from SEM images is larger than the crystallite size calculated using XRD measurement, which indicates that each grain is formed by aggregation of number of nanocrystals. The larger grain size of $Ni_{0.7}Co_{0.3}Fe_2O_4$ compared to $NiFe_2O_4$ sample is in agreement with XRD results.

3.2. Impedance spectroscopy

The frequency dependent real (Z') and imaginary (Z'') parts of the impedance at room temperature for the sintered $NiFe_2O_4$ and $Ni_{0.7}Co_{0.3}Fe_2O_4$ ceramics are presented in Figs. 4 and 5, respectively. The high values of real part of the impedance (Z') at low frequency region are due to long range motion of ions in the material and the electrode effects. The magnitude of Z' starts to decrease with the frequency increase due to the short range motion of the ions. It is noticed (Figs. 4 and 5) that the Co-doped sample ($Ni_{0.7}Co_{0.3}Fe_2O_4$) has higher impedance (Z' and Z'') than the pure $NiFe_2O_4$, which is due to the redistribution of cations and the hopping mechanism.

3.3. Dielectric properties

The dielectric properties (permittivity, ε' and dielectric loss, $\tan\delta$) of polycrystalline materials are generally determined by a combination of various factors like

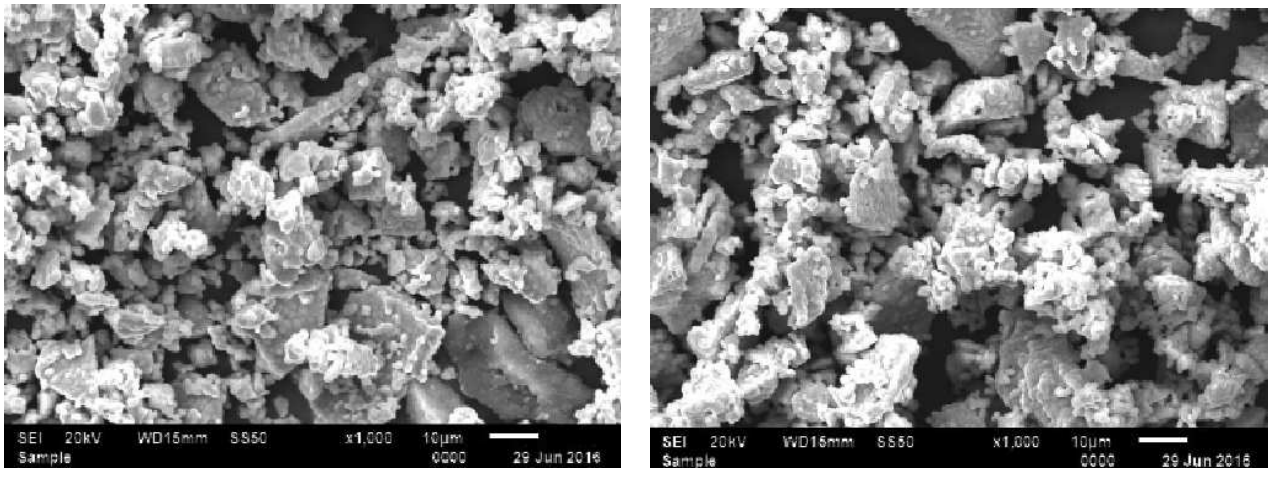

(a) (b)

Figure 3. SEM micrographs of calcined powders: a) $NiFe_2O_4$ and b) $Ni_{0.7}Co_{0.3}Fe_2O_4$

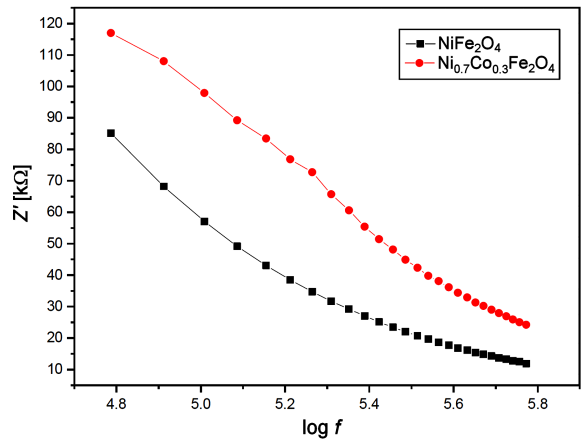

Figure 4. Variation of real part of impedance (Z') with frequency for $NiFe_2O_4$ and $Ni_{0.7}Co_{0.3}Fe_2O_4$

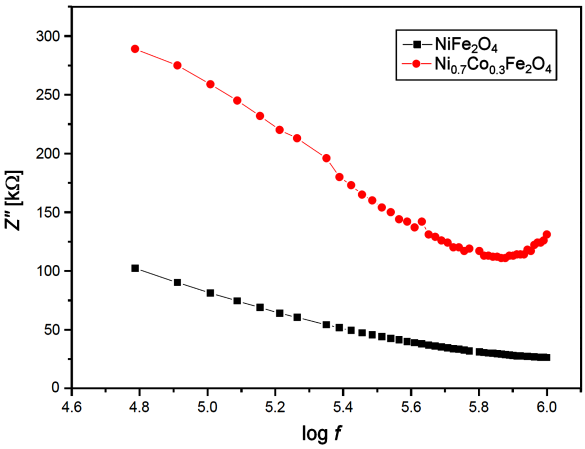

Figure 5. Variation of imaginary part of impedance (Z'') with frequency for $NiFe_2O_4$ and $Ni_{0.7}Co_{0.3}Fe_2O_4$

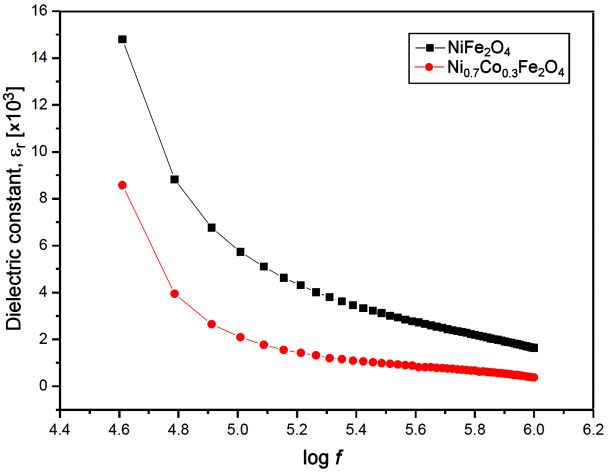

Figure 6. Variation of electric permittivity with log frequency for $NiFe_2O_4$ and $Ni_{0.7}Co_{0.3}Fe_2O_4$

method of preparation, sintering temperature, substitution used, the ratio of Fe^{3+}/Fe^{2+} ions and AC conductivity.

The electric permittivity was calculated by using following formula:

$$\varepsilon' = \frac{C \cdot d}{\varepsilon_0 \cdot A} \tag{1}$$

where C is the measured capacitance, d is the thickness of the sample, A is the area of the pellet and ε_0 is the permittivity of free space (8.85×10^{-12} F/m). The frequency dependence of the real part of electric permittivity (ε') for $NiFe_2O_4$ and $Ni_{0.7}Co_{0.3}Fe_2O_4$ compounds measured at room temperature in the frequency range of 20 Hz–1 MHz is shown in Fig. 6. It is evident that the dielectric permittivity initially decreases sharply with increasing frequency. At higher frequencies, it decreases slowly and becomes almost constant. This is due to the fact that the species contributing to the polarizability are lagging behind the applied field at higher frequency. The observed decrease of ε' for $NiFe_2O_4$ and $Ni_{0.7}Co_{0.3}Fe_2O_4$ is caused by various types of polarizations [19–21]. The larger value of (ε') at lower frequencies is mainly due to the contributions from polarizations of ionic, space charge/interface and grain boundaries. The decrease in orientation polarizability with increasing frequency may be responsible for the decrease in (ε_r) at higher frequencies. Since more than one ion (O^{2-}, Fe^{3+}, Ni^{2+} and Co^{2+}) contributes to the relaxation process, the data were fitted to the modified Debye's function that considers the possibility of more than one ion contributing to the relaxation [22].

The energy loss is generally characterized by the dielectric loss factor $\tan\delta = \varepsilon''/\varepsilon'$, where the angle δ is the phase difference between applied electric field and induced current. Dielectric loss arises if the polarization lags behind the applied alternating field which may be caused by grain boundaries, impurities and imperfections in the crystal [23]. The density of a material is also responsible for the variation in dielectric loss. Low density results in low dielectric constant and higher dielectric loss [24]. Figure 7 shows the variation of $\tan\delta$ with frequencies in $NiFe_2O_4$ and $Ni_{0.7}Co_{0.3}Fe_2O_4$ compounds at room temperature. Continuous decrease of $\tan\delta$ can be seen for both samples. The decrease in the values of dielectric loss (and permittivity too) with frequency can be related to electron exchange interaction between Fe^{2+} and Fe^{3+} ions which cannot follow the alternation of the electric field beyond a certain frequency in $NiFe_2O_4$. In addition, the pure $NiFe_2O_4$ has higher permittivity and dielectric loss in comparison to $Ni_{0.7}Co_{0.3}Fe_2O_4$.

3.4. AC conductivity

The AC conductivity was calculated from dielectric data using the relation:

$$\sigma_{AC} = \omega \cdot \varepsilon_r \cdot \varepsilon_0 \cdot \tan\delta \tag{2}$$

where $\omega = 2\pi \cdot f$. The frequency dependent AC conductivity (σ_{AC}) for $NiFe_2O_4$ and $Ni_{0.7}Co_{0.3}Fe_2O_4$ ferrites measured at room temperature is shown in Fig. 8. It is evident that the conductivity of $Ni_{0.7}Co_{0.3}Fe_2O_4$ is almost constant, but in the case of $NiFe_2O_4$ a slight in-

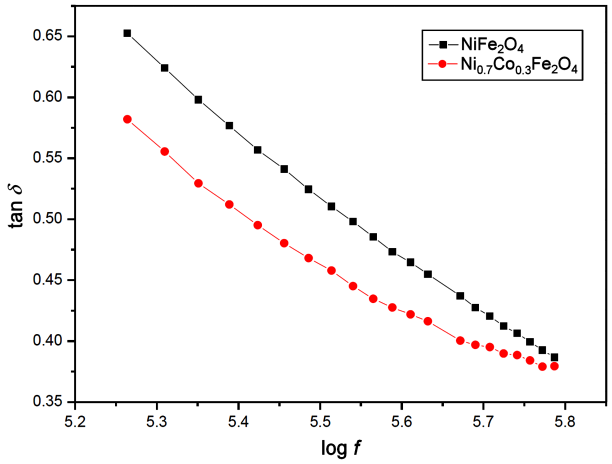

Figure 7. Variation of dielectric loss with log frequency for $NiFe_2O_4$ and $Ni_{0.7}Co_{0.3}Fe_2O_4$

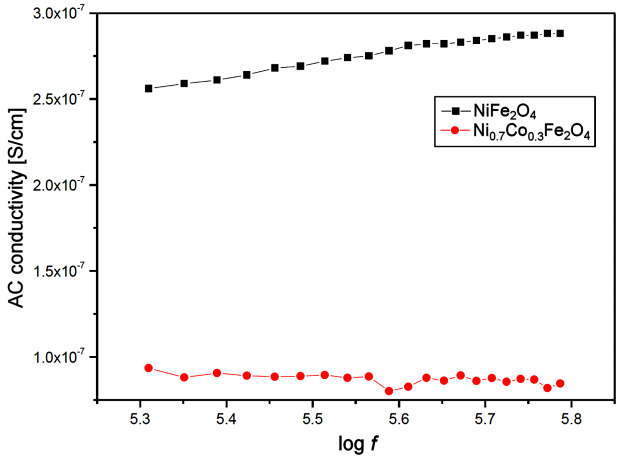

Figure 8. Variation of AC conductivity with log frequency for $NiFe_2O_4$ and $Ni_{0.7}Co_{0.3}Fe_2O_4$

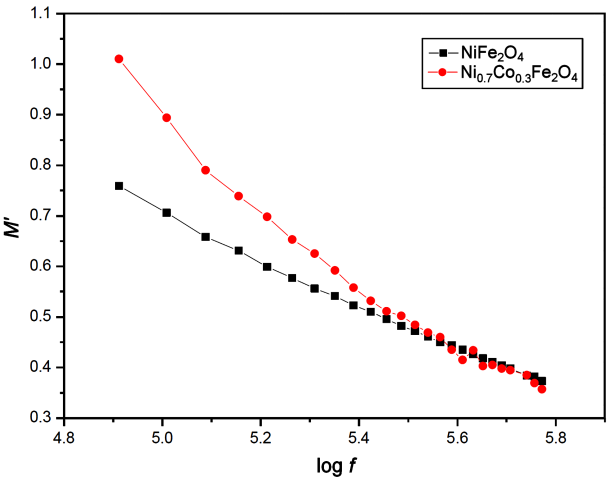

Figure 9. Variation of real modulus (M') with frequency for $NiFe_2O_4$ and $Ni_{0.7}Co_{0.3}Fe_2O_4$

crease in the conductivity with frequency might be seen (Fig. 8). The frequency dependent AC electrical conductivity of ferrites is generally accepted to be due to the electron hopping between Fe^{2+} and Fe^{3+} ions on the octahedral sites. In the present case, the observed increase in σ_{AC} with increasing frequency for $NiFe_2O_4$ can be attributed to the increased hopping rate with increasing frequency. It is also evident that the AC conductivity at room temperature of $NiFe_2O_4$ is somewhat higher than for $Ni_{0.7}Co_{0.3}Fe_2O_4$ (Fig. 8) which is in accordance with literature data [25,26].

3.5. Electric modulus

The complex electric modulus spectra represent the measure of the distribution of ion energies or configurations in the structure and also describe the electrical relaxation of ion conducting lattices as a microscopic property of materials. The real (M') and imaginary (M'') parts of electric modulus (M^*) were calculated using the real and imaginary parts of impedance data measured at different frequencies for both $NiFe_2O_4$ and $Ni_{0.7}Co_{0.3}Fe_2O_4$ samples. The variation of the real part of electric modulus as function of frequency with frequency range (20 Hz–1 MHz) at room temperature for $NiFe_2O_4$ and $Ni_{0.7}Co_{0.3}Fe_2O_4$ samples is shown in Fig. 9. The real part of electric modulus decreases with frequency without any characteristic peak in the measured frequency region [27,28].

3.6. ESR Spectra

The ESR spectra of ferrites are important for investigating the magnetic properties of magnetic materials at high frequency because the resonance originates from the interaction between spin and electromagnetic waves. The powder ESR spectra of $NiFe_2O_4$ and $Ni_{0.7}Co_{0.3}Fe_2O_4$ are measured at 650 mT at room temperature and are shown in Fig. 10. It can be seen that the g-value varies with cobalt substitution. This decrease in the g-value may be due to the super exchange interaction between Ni^{2+} and Fe^{3+} ions through non-magnetic O^{2-} ions. The super exchange interaction in ferrite is responsible for magnetic ordering within each sub-lattice. The interaction between A and B site is strong in ferrites. As the AB interaction predominate, the spins of A

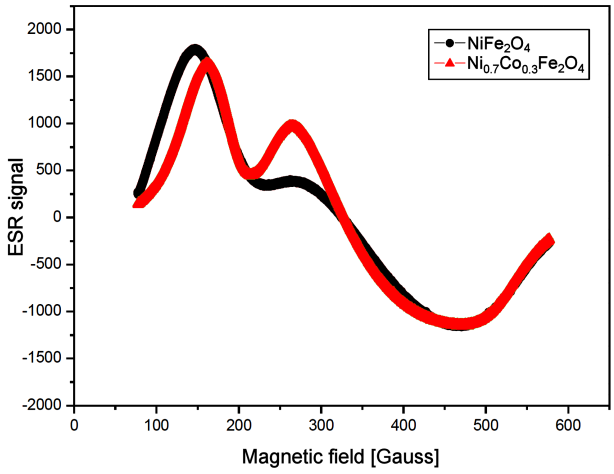

Figure 10. ESR spectra of $NiFe_2O_4$ and $Ni_{0.7}Co_{0.3}Fe_2O_4$ ferrites

and B site ions in ferrites will be opposite with a resultant magnetic moment equal to the difference between those of A and B site ions [28,29].

IV. Conclusions

The $NiFe_2O_4$ and $Ni_{0.7}Co_{0.3}Fe_2O_4$ spinel ferrites have been synthesised successfully using sol-gel method and pressed and sintered at 1200 °C. The XRD patterns showed that both ferrites have single spinel phase. The lattice parameter of $Ni_{0.7}Co_{0.3}Fe_2O_4$ is larger than $NiFe_2O_4$. The FTIR spectra show the mixed spinel nature of nickel ferrite. The decrease in dielectric constant and increase in the conductivity with frequency is required for high frequency applications. The obtained results are well compared with previous literature and they will be encouraging for further studies like VSM, Mossbauer spectra etc.

References

1. Z. Lazarevic, C. Jovalekic, A. Milutinovic, M.J. Romcevic, N.Z. Romcevic, "Preparation and characterization of nano ferrites", *Acta Phys. Pol. A*, **121** (2012) 682–686.
2. L. Gama, A.P. Dinaz, A.C.F.M. Costa, S.M. Bezende, A. Azevedo, D.R. Cornejo, "Magnetic properties of nanocrystalline Ni-Zn ferrites doped with samarium", *Physica B: Condensed Matter*, **384** (2006) 97–99.
3. H.S. Mund, Shailja Tiwari, Jagrati Sahariya, M. Itou, Y. Sakurai Y, B.L. Ahuja, "Investigation of orbital magnetization in inverse spinel cobalt ferrite using magnetic Compton scattering", *J. Appl. Phys.*, **110** (2011) 073914.
4. A.B. Gadkari, T.J. Shinde, P.N. Vasambekar, "Structural analysis of Y^{3+} doped Mg-Cd ferrites prepared by oxalate co-precipitation method", *Mater. Chem. Phys.*, **114** (2009) 505–510.
5. S. Bhukal, T. Namgyal, S. Mor, S. Bansal, S. Singhal, "Structural, electrical, optical and magnetic properties of chromium substituted Co-Zn nanoferrites $Co_{0.6}Zn_{0.4}Cr_xFe_{2-x}O_4$ ($0 \le x \le 1.0$) prepared via sol-gel auto-combustion method", *J. Mol. Struct.*, **1012** (2012) 162–167.
6. I. Sharifi, H. Shokrollahi, "Nanostructural, magnetic and Mossbauer studies of nanosized $Co_{1-x}Zn_xFe_2O_4$ synthesized by co-precipitation", *J. Magn. Magn. Mater.*, **324** (2012) 2397–2403.
7. S.E. Jcoba, S. Dukalde, H.R. Bertorella, "Rare earth influence on the structural and magnetic properties of NiZn ferrites", *J. Magn. Magn. Mater.*, **272** (2004) 2253–2254.
8. D.H. Chen, X.R. He, "Synthesis of nickel ferrite nanoparticles by sol-gel method", *Mater. Res. Bull.*, **36** (2001) 1369–1377.
9. Y. Shi, J. Ding, X. Liu, J. Wang, "$NiFe_2O_4$ ultrafine particles prepared by co-precipitation/mechanical alloying", *J. Magn. Magn. Mater.*, **205** (1999) 249–254.
10. M.S. Al-Hoshan, J.P. Singh, A.M. Al-Mayouf, A.A. Al-Suhybani, M.N.Shaddad, "Synthesis, physicochemical and electrochemical properties of nickel ferrite spinels obtained by hydrothermal method for the oxygen evolution reaction (OER)", *Int. J. Electrochem. Sci.*, **7** (2012) 4959–4973.
11. S.A. Morrison, C.L. Cahill, E.E. Carpenter, S. Calvin, R.S. Waminnathon, M.E. McHenry, V.G. Harris, "Magnetic and structural properties of nickel zinc ferrite nanoparticles synthesized at room temperature", *J. Appl. Phys.*, **95** (2004) 6392–6395.
12. R. Sen, P. Jain, R. Patidar, S. Srivastava, R.S. Rana, N. Gupta, "Synthesis and Characterization of nickel ferrite ($NiFe_2O_4$) nanoparticles prepared by sol-gel method", *Mater. Today*, **2** [4-5] (2015) 3750–3757.
13. T. Shanmugavel, S. Gokul Raj, G. Ramesh Kumar, G. Rajarajan, D. Saravanan, "Cost effective preparation and characterization of nanocrystalline nickel ferrites ($NiFe_2O_4$) in low temperature regime", *J. King Saud Univer. Sci.*, **27** (2015) 176–181.
14. A. Sutka, G. Mezinskis, "Sol-gel auto-combustion synthesis of spinel-type ferrite nanomaterials", *Frontiers Mater. Sci.*, **6** (2012) 128–141.
15. R.D. Shannon, "Revised effective ionic radii and systematic studies of interatomic distances in halides and chalcogenides", *Acta Crystall. A*, **32** (1976) 751–767.
16. P.D. Thang, G. Rijinders, D.H.A. Blank, "Spinel cobalt ferrite by complexometric synthesis", *J. Magn. Magn. Mater.*, **295** (2005) 251–256.
17. T. Shanmugavel, S. Gokul Raj, G. Rajarajan, G. Ramesh Kumar, "Tailoring the structural and magnetic properties and of nickel ferrite by auto combustion method", *Procedia Mater. Sci.*, **6** (2014) 1725–1730.
18. O.M. Hemeda, M.M. Barakat, D.M. Hemada, "Structural, electrical and spectral studies on double rare-earth orthoferrites $La_{1-x}Nd_xFeO_3$", *Turk. J. Phys.*, **27** (2003) 537–549.
19. T. Shanmugavel, S. Gokul Raj, G. Rajarajan, G. Ramesh Kumar, G. Boopathi, "Combustion synthesis and structural analysis of nanocrystalline nickel ferrite at low temperature regime. Synthesis, characterization and magnetic properties of nanocrystalline nickel", *AIP Conf. Proceedings*, **1665** (2015) 050182.
20. N. Ponpandian, A. Narayanasamy, "Influence of grain size and structural changes on the electrical properties of nanocrystalline zinc ferrite", *J. Appl. Phys.*, **92** (2002) 2770–2778.
21. S. Omprakash, A.P. Gnana Prakash, P.S. Naik, "AC conductivity and dielectric studies on nickel ferrite nanoparticles synthesized by sol gel technique", *16th International Workshop on Physics of Semiconductor Devices*, 85491S, 2012 (doi:10.1117/12.925306).
22. J.C. Anderson, *Dielectrics*, Spottiswoode, Ballantyne & Co Ltd., London and Colchester, 1964.
23. A. Verma, O.P. Thakur, C. Prakash, T.C. Goel, R.G. Mendiratta, "Temperature dependence of electrical properties of nickel-zinc ferrites processed by the citrate precursor technique", *Mater. Sci. Eng. B*, **116** (2005) 1–6.
24. Md.T. Rahman, M. Vargas, C.V. Ramana, "Structural characteristics, electrical conduction and dielectric properties of gadolinium substituted cobalt ferrite", *J. Alloys Compd.*, **617** (2014) 547–562.
25. R.V. Mangalaraja, P. Manohar, F.D. Gnanam, "Electrical and magnetic properties of $Ni_{0.8}Zn_{0.2}Fe_2O_4$/silica composite prepared by sol-gel method", *J. Mater. Sci.*, **39** (2004) 2037–2042.
26. R. Bhandare, H.V. Jamadar, A.T. Pathan, B.K. Chougule, A.M. Shaikh, "Dielectric properties of Cu substituted $Ni_{0.5-x}Zn_{0.3}Mg_{0.2}Fe_2O_4$ ferrites", *J. Alloys Compd.*, **509** (2011) L113–L118.

27. P. Muralidharan, N. Nallamuthu, I. Prakash, N. Satyanarayana, M. Venkateswarlu, "AC conductivity and electrical modulus studies on lithium vanadophosphate glasses", *J. Am. Ceram. Soc.*, **90** (2007) 125–131.
28. K. Anand, B. Ramamurthy, V. Veeraiah, K. Vijaya Babu, "Structural, dielectric and conductivity studies of $LiNi_{0.75}Mg_{0.25-x}Cu_xPO_4$ synthesized by solid state reaction method", *Process. Appl. Ceram.*, **10** [1] (2016) 47–55.
29. P. Priyadharsini, A. Pradeep, P.S. Rao, G. Chandrasekaran, "Structural, spectroscopic and magnetic study of nanocrystalline Ni-Zn ferrites", *Mater. Chem. Phys.*, **116** (2009) 207–213.
30. N.M. Deraz, A. Alarifi, "Controlled synthesis, physicochemical and magnetic properties of nano-crystalline Mn ferrite system", *Int. J. Electrochem. Sci.*, **7** (2012) 5534–5543.